7th International Conference on Multiphase Flow,
ICMF 2010, Tampa, FL, May 30 – June 4, 2010

A VOF method coupled with a dynamic contact angle model for simulation of two-phase flows with partial wetting

Bogdan A. Nichita[a] , Iztok Zun[b] and John R. Thome[a]

[a] EPFL STI IGM LTCM, ME G1 464, Station 9, CH-1015 Lausanne, SWITZERLAND

[b] LFDT, Faculty of Mechanical Engineering, University of Ljubljana, Askerceva 6, 1000 Ljubljana, SLOVENIA

bogdan.nichita@epfl.ch, iztok.zun@fs.uni-lj.si and john.thome@epfl.ch

Keywords: volume-of-fluid, contact angle, advancing, receding, FLUENT

Abstract

This paper describes the development and the implementation of a 3D dynamic contact angle model into the VOF method provided by the commercial CFD code FLUENT for simulations of two phase flows with wetted boundaries. At present, FLUENT only allows user specified fixed values for the contact angle. This is physically quite limiting and leads to non-realistic interfacial effects for these applications. The contact angle becomes important in problems where the surface tension forces are more significant than the inertial forces. Problems are also encountered where dry patches are formed on channel walls, which give rise to a triple point between the wall, the liquid and the gas. This is often the case for two phase flows inside micro and mini channels. In FLUENT, the contact angle, which the fluid is assumed to make with the wall, is used to adjust the surface normal vector to the interface in cells near the wall. This so-called dynamic boundary condition results in the adjustment of the curvature of the interface near the wall. In our model, the 3D contact angle is computed based on the volume fraction and the contact line velocity, and is limited by the experimentally available advancing and receding static contact angles. Several 2D and 3D tests are presented, which demonstrate the accuracy of our model.

Introduction

Two phase flows have been widely studied over the last years both numerically and experimentally. From the point of view of numerics, a large amount of work has been done regarding the so called "one" fluid models, where a single set of conservation equations is solved for the whole domain and the interface is then tracked or captured.

Interface tracking techniques explicitly track the interface with marker particles like in MAC methods (Harlow & Welch 1965), arbitrary Lagrangian-Eulerian (ALE) methods (Donea 1983; Hirt *et al.* 1997; Hughes *et al.* 1991), or front tracking methods (Tryggvason *et al.* 2001; Unverdi & Tryggvason 1992). These interface tracking methods are very accurate and efficient for flexible moving boundaries with small deformations. However their main drawback is that they are difficult to use in cases where the interface breaks up or coalesces with another interface. Also additional re-meshing is needed when a large deformation of the interface occurs.

In interface capturing methods, an auxiliary function is needed. These methods are very robust and have a wide range of applicability. However, they require higher mesh resolutions. Examples include volume of fluid (VOF) (Hirt & Nichols 1981; Youngs 1992; Li 1995; Scardovelly & Zaleski 1999) and level set methods (Sussman *et al.* 1994, 1998, 1999; Sussman & Fatemi 1999).

In VOF methods, the interface is given implicitly by a color function, which is defined as the volume fraction of one of the fluids within each cell. From this function, a reconstruction of the interface is made and the interface is then propagated implicitly by updating the color function. VOF methods are conservative and can deal with topological changes of the interface. However, VOF methods cannot accurately compute several important properties, such as curvature and the normal to the interface. Moreover, a high order of accuracy is hard to achieve because of the discontinuities in the color function.

For two phase flows in microchannels, the surface tension forces play an important role in determining the dynamics of bubbles whereas gravitational forces are generally less important, if not negligible. Also it is very important to consider the interaction between the boundaries and the fluids by prescribing or computing the correct contact angle between the interface and the boundary. FLUENT allows one to input either a static value for the contact angle, or to use User Defined Functions (UDF) to compute the dynamic contact angle. When the contact line starts to move, a fix static value of the contact angle would be inappropriate to use. Therefore the use of a dynamic contact angle model is much more in-

dicated.

In this paper we propose a 3D dynamic contact angle model based on volume fraction, interface reconstruction, and advancing and receding static contact angles available experimentally. To define the advancing contact angle, one needs to dynamically add volume to the liquid-phase to determine the maximum volume permitted without increasing the interfacial area between the liquid and solid phases. For the definition of the receding contact angle, one needs to remove volume from the liquid-phase to the minimum volume permitted without decreasing the interfacial area between the liquid and solid phases. These two angles refer to the static values. When the contact line starts to move, the contact angles will deviate from their equilibrium value to provide the dynamic advancing and receding contact angles.

The rest of this paper is organized as follows: section 2 presents the dynamic contact angle model with all the geometrical considerations, section 3 briefly outlines the FLUENT discretization procedure and code development, section 4 presents several numerical validation tests, and conclusions are given in section 5.

Mathematical formulation

If the surface tension is assumed constant between each pair of the three phases (liquid, gas and solid), see Fig. 1 Young's equation reads as:

$$\sigma_{LG}\cos\theta_s = \sigma_{GS} - \sigma_{LS} \tag{1}$$

In Eq. 1, θ_s is the static contact angle, σ_{LG} is the liquid-gas surface tension, σ_{LS} is the solid-liquid surface tension, and σ_{GS} is the gas-solid surface tension. The real dynamic contact angle can take any value within the interval $\theta_R \leq \theta \leq \theta_A$, where θ_R and θ_A are the dynamic receding and the dynamic advancing contact angles. To compute these values, we used the correlation of Tanner (Tanner 1979) for the receding angle, see Eq. 2, and the correlation of Jiang *et al.* (Jiang *et al.* 1979) for the advancing angle, see Eq. 3:

$$\theta_{rec,s}^3 - \theta_R^3 = 72Ca \tag{2}$$

$$\frac{\cos\theta_{adv,s} - \cos\theta_A}{\cos\theta_{adv,s} + 1} = \tanh\left(4.96Ca^{0.702}\right) \tag{3}$$

In Eq. 2, θ_R is the dynamic receding contact angle and $\theta_{rec,s}$ is the static receding contact angle. In Eq. 3, θ_A is the dynamic advancing contact angle and $\theta_{adv,s}$ is the static advancing contact angle. In both Eq. 2 and Eq. 3, Ca is the capillarity number given by:

$$Ca = \frac{\mu v}{\sigma} \tag{4}$$

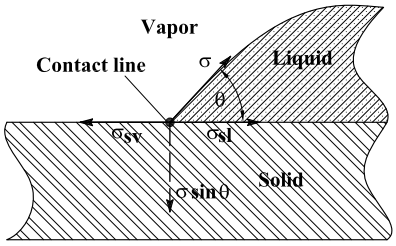

Figure 1: Equilibrium contact line and contact angle.

where in Eq. 4 μ is the dynamic viscosity of the liquid, v is the contact line velocity and σ is the liquid-gas surface tension.

Once the upper and the lower limits of the contact angle are calculated, we evaluated the dynamic contact angle based on the geometrical reconstruction of the interface. We now give some details about the VOF method used by FLUENT to capture the interface.

The volume of fluid method. The basic idea of the VOF method is to consider a color function, defined as the volume fraction of one of the fluids within each cell, to capture the interface. This function will be unity if the cell is filled with the gas phase, zero if the cell is filled with the liquid phase and between zero and one if the cell contains the interface. VOF belongs to the so called "one" fluid family of methods, where a single set of conservation equations is solved for the domain:

$$\frac{\partial(\rho\mathbf{u})}{\partial t} + \nabla\cdot(\rho\mathbf{u}\otimes\mathbf{u}) = -\nabla p + \nabla\cdot(2\mu\mathbf{D}) + \mathbf{F}_{st} + \rho\mathbf{g} \tag{5}$$

$$\frac{\partial\rho}{\partial t} + \nabla\cdot(\rho\mathbf{u}) = 0 \tag{6}$$

In Eq. 5 and Eq. 6, $\mathbf{u}$ is the velocity vector, ρ is the density, t is the time, μ is the dynamic viscosity, $\mathbf{D}$ is the rate of deformation tensor with the components $D_{ij} = \frac{1}{2}(u_{i,j} + u_{j,i})$, $\mathbf{F}_{st}$ is the body force due to the surface tension, and $\mathbf{g}$ is the gravity vector.

In VOF, the density and the dynamic viscosity are described by the following formulae:

$$\rho(\mathbf{x},t) = \rho_l + (\rho_g - \rho_f)F$$

$$\mu(\mathbf{x},t) = \mu_l + (\mu_g - \mu_l)F$$

where the subscripts l and g denote liquid and gas phases, respectively.

After solving Eq. 5 and Eq. 6, the color function is advected with the velocity field by:

$$\frac{\partial F}{\partial t} + \mathbf{u}\cdot\nabla F = 0 \tag{7}$$

In general, a VOF algorithm solves the problem of updating the volume fraction field F given the fixed grid, the velocity field $\mathbf{u}$ and the field F at the previous step. In two dimensions, the interface is considered to be a continuous piecewise smooth line, and the problem of its reconstruction is that of finding the approximation to the section of the interface in each cell, by knowing only the volume fraction F in that cell and in the neighboring cells. The simplest type of VOF methods are the Simple Line Interface Calculation (SLIC) (Noh & Woodward 1976) or the SOLA-VOF algorithm (Hirt & Nichols 1981). They are first order accurate in the reconstruction of the interface. Typically, the reconstructed interface is made up of a sequence of segments aligned with the grid. Fig. 2 shows the exact color VOF function for a smooth circular arc, whilst Fig. (3(a)) shows the interface reconstruction using SLIC method. More accurate VOF techniques attempt to fit the interface with piecewise linear segments. These are known as Piecewise Linear Interface Calculation (PLIC) (Li 1995); Fig. 3(b) shows an interface reconstructed with VOF/PLIC.

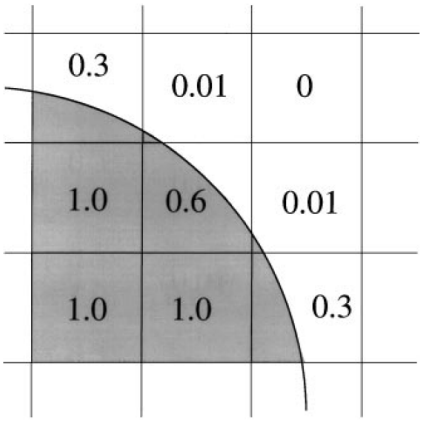

Figure 2: The exact VOF color function for a circular arc over a square grid.

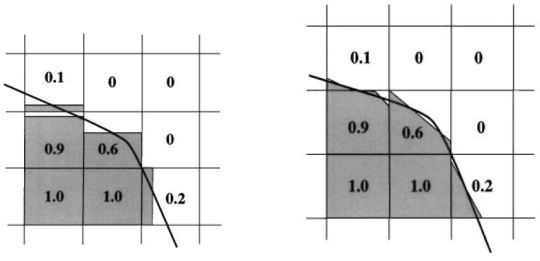

(a) SLIC (b) PLIC

Figure 3: Interface reconstruction schemes.

Because F in Eq. 7 is not a continuous function, the VOF/PLIC algorithm is divided into two parts: a reconstruction step and a propagation step. The key part of the reconstruction step is the determination of the orientation of the segment. This is equivalent to the determination of the unit normal vector $\mathbf{n}$ to the segment. The normal vector $\mathbf{n}$ and the volume fraction F then uniquely determine the straight line. The second step of the VOF algorithm is the propagation. Usually, the propagation step is done using a fractional step or an operator split method, which updates the volume fraction F by advecting the interface along one spatial direction at a time. Intermediate F values are calculated during this process, and the final F field is obtained only after advection of the interface along all coordinate directions. Although they are more complicated, unsplit methods exist as well.

The surface tension term in Eq 5 is approximated using the Continuum Surface Force model of Brackbill *et al.* (Brackbill *et al.* 1992) given by the following relation:

$$F_{st} = \frac{\rho k \nabla F}{\frac{1}{2}(\rho_l + \rho_g)} \tag{8}$$

where in Eq. 8 ρ is the discontinuous density, k is the curvature of the interface, and ρ_l and ρ_g are the liquid and , the gas densities respectively.

The contact angle model. A first step in determining the contact angle between the interface and boundary is similar to the reconstruction step from the advection algorithm of the volume fraction F. Given the normal vector to the interface $\mathbf{m} = [m1, m2, m3]$, the equation of the interface, which is a plane in 3D and a line in 2D, is given by:

$$m1x + m2y + m3z = \alpha \tag{9}$$

where in Eq. 9 α is the plane constant (line in 2D). Scardovelli and Zaleski (Scardovelly & Zaleski 1999) presented analytical relations for determining α. Once the plane constant α is determined, we used the same relation which connects α with the volume fraction F to express the contact angle, and the following notations like as in (Fang *et al.* 2008) $g = m_2/m_1$, $h = \alpha/m_1$, $f = m_3/m_1$. For 3D we get:

$$F = \frac{1}{6gf}\left[h^3 - \sum_{i=1}^{3} H\left(h - \frac{m_i \Delta x_i}{m_1}\right)\left(h - \frac{m_i \Delta x_i}{m_1}\right)^3 + \sum_{i=1}^{3} H\left(h - \Delta x_1 - g\Delta x_2 - f\Delta x_3 + \frac{m_i \Delta x_i}{m_1}\right)\left(h - \Delta x_1 - g\Delta x_2 - f\Delta x_3 + \frac{m_i \Delta x_i}{m_1}\right)^3\right] \tag{10}$$

where in Eq. 10 H is the discontinuous Heaviside function. For 2D Eq. 10 becomes:

$$F = \frac{1}{2g}\left[h^2 - \sum_{i=1}^{2} H\left(h - \frac{m_i \Delta x_i}{m_1}\right)\left(h - \frac{m_i \Delta x_i}{m_1}\right)^2\right] \tag{11}$$

Now observing that $\tan(\theta) = \sqrt{m_1^2 + m_2^2}/m_3$, Eq. 10 becomes:

$$F = \frac{\tan\theta}{6g\sqrt{1+g^2}} \left[h^3 - \sum_{i=1}^{3} H\left(h - \frac{m_i \Delta x_i}{m_1}\right)\left(h - \frac{m_i \Delta x_i}{m_1}\right)^3 + \sum_{i=1}^{3} H\left(h - \Delta x_1 - g\Delta x_2 - \frac{\sqrt{1+g^2}}{\tan\theta}\Delta x_3 + \frac{m_i \Delta x_i}{m_1}\right) \left(h - \Delta x_1 - g\Delta x_2 - \frac{\sqrt{1+g^2}}{\tan\theta}\Delta x_3 + \frac{m_i \Delta x_i}{m_1}\right)^3 \right] \quad (12)$$

For the 2D case we have $\tan(\theta) = m_1/m_2$ so Eq. 11 becomes:

$$F = \frac{\tan(\theta)}{2} \left[h^2 - \sum_{i=1}^{2} H\left(h - \frac{m_i \Delta x_i}{m_1}\right)\left(h - \frac{m_i \Delta x_i}{m_1}\right)^2 \right] \quad (13)$$

Eq. 12 and Eq. 13 are solved iteratively for θ with a Newton iterative method. The derivative of Eq. 12 with respect to θ is given by:

$$\frac{\partial F}{\partial \theta} = A + B + C \quad (14)$$

In Eq. 14 A, B and C are given by the following relations:

$$A = \frac{1}{6g\sqrt{1+g^2}\cos^2\theta} \left[h^3 - \sum_{i=1}^{3} H\left(h - \frac{m_i \Delta x_i}{m_1}\right) \left(h - \frac{m_i \Delta x_i}{m_1}\right)^3 + \sum_{i=1}^{3} H\left(h - \Delta x_1 - g\Delta x_2 - \frac{\sqrt{1+g^2}}{\tan\theta}\Delta x_3 + \frac{m_i \Delta x_i}{m_1}\right) \left(h - \Delta x_1 - g\Delta x_2 - \frac{\sqrt{1+g^2}}{\tan\theta}\Delta x_3 + \frac{m_i \Delta x_i}{m_1}\right)^3 \right] \quad (15a)$$

$$B = -\frac{\tan\theta}{2g\sin^2\theta} \left[H(h-f)\left(h - \frac{\sqrt{1+g^2}}{\tan\theta}\right)^2 \right] \quad (15b)$$

$$C = \frac{\tan\theta}{2g\sin^2\theta} \left[H(h-g-f)\left(h - g - \frac{\sqrt{1+g^2}}{\tan\theta}\right)^2 + H(h-1-f)\left(h - 1 - \frac{\sqrt{1+g^2}}{\tan\theta}\right)^2 \right] \quad (15c)$$

For the 2D case A, B and C in Eq. 14 have the following form:

$$A = \frac{1}{2\cos^2\theta} \left[h^2 - \sum_{i=1}^{2} H\left(h - \frac{m_i \Delta x_i}{m_1}\right)\left(h - \frac{m_i \Delta x_i}{m_1}\right)^2 \right] \quad (16a)$$

$$B = -\frac{\tan\theta}{\sin^2\theta} H(h-g)\left(h - \frac{1}{\tan\theta}\right) \quad (16b)$$

$$C = 0.0 \quad (16c)$$

To summarize, the following algorithm was followed:

- for the cell containing the interface, compute the plane (line) constant α;
- by knowing the position at the current time step and at the previous time step, a contact line velocity can be rapidly computed;
- with the contact line velocity known, the dynamic advancing and dynamic receding contact angles can be computed using Eq. 3 and Eq. 2 using the input values of static advancing and static receding contact angles;
- the dynamic contact angle is then computed using Eq. 12 (or Eq. 13 for the 2D case) and if the value falls between the receding and advancing angles, then this value will be returned to the FLUENT solver, otherwise the advancing or the receding angle is returned to the FLUENT solver;
- move to the next time step.

FLUENT discretization and code development

FLUENT is a finite volume code, so one needs to solve the integral form of Eq. 7 which in conservative form reads as:

$$\int_V \frac{\partial \rho F}{\partial t} + \int_V \nabla \cdot (\rho \mathbf{u} F) = 0 \quad (17)$$

For the unsteady term, FLUENT employs first order Euler discretization. For the convective term, the Green-Gauss theorem is applied and the volume integral is transformed into a surface integral.

FLUENT uses a mid-point rule integration of the surface integral which is second-order accurate. It also provides five schemes to interpolate the face values F_f, namely: first order upwind, second order upwind, power law, QUICK, and MUSCL. Because the MUSCL (Monotone Upwind Schemes for Conservative Laws) scheme is less diffusive than the others, it was used in all our numerical applications to interpolate face values in Eq. 7 and Eq. 5. In Eq. 5, if the pressure field is known, one can solve for the velocity field. However, the pressure field is not known *a priori* and must be obtained as part of the solution. FLUENT offers several pressure-velocity coupling algorithms like SIMPLE (Semi-Implicit Pressure Linked Equations), SIMPLEC (SIMPLE Consistent), and PISO (Pressure Implicit with Split of Operators). Since FLUENT uses a collocated grid where pressure and velocity are stored at cell-centers, an interpolation procedure is needed to interpolate the pressure face values from the cell-center values. For two-phase flow, FLUENT provides two schemes,

namely body-force-weighted which computes the pressure by assuming that the normal gradient of the difference between pressure and body forces is constant, and PRESTO! (PREssure STaggering Option) which uses the discrete continuity balance for a "staggered" control volume about the face to compute the face pressure. In all our simulations the PISO scheme was used for the velocity-pressure coupling, and the PRESTO! scheme for the pressure interpolation.

In FLUENT the dynamic contact angle model was implemented using User Defined Functions. The values of the contact angle and other parameters are stored for the current and the previous time step, for handling the situation when the contact line is shifting from one cell to another. Once the contact angle is computed and returned to the FLUENT solver, the surface normal at the live cell next to the wall is:

$$\mathbf{n} = n_w \cos\theta + n_t \sin\theta \tag{18}$$

where in Eq. 18 n_w and n_t are the unit vectors normal and tangential to the wall, respectively.

Numerical validations

In this section several 2D and 3D simulations are presented for air-water and a coated silicon wafer surface.

2D examples. In the present study, a semi-circular droplet of 2cm diameter is placed on a wall of a rectangular domain of 8x2.5cm at (4.0,0.5) cm with a gravity vector $(0.0, -9.81)\ m/s^2$. The fluids used are air and water, see Table 1 for their physical properties. Fang *et al.* (Fang *et al.* 2008) have measured the contact angle for air-water on a coated silicon wafer surface and found that the advancing contact angle is around 105° and that the receding contact angle is around 65°. Consequently, in our simulations we used the above mentioned values as limiters for the dynamic contact angle. A no slip wall boundary condition was used for all boundaries. Besides this, for the bottom boundary the dynamic contact angle was computed and prescribed. Three different grids were used: 80x25, 160x50 and 320x100. Fig 4 shows the bubble contour at different times using a grid of 80x25. Fig. 5 and Fig. 6 show the bubble contour on a grid of 160x50 and on a grid of 320x100, respectively. Similar shapes were found numerically by Manservisi and Scardovelli (Manservisi & Scardovelli 2008) and experimentally by Lim *et al.* (Lim *et al.* 2008) and Grundke *et al.* (Grundke *et al.* 2008). Grundke *et al.* (Grundke *et al.* 2008) measured a contact angle between a sessile water drop and a silicone surface between 70° and 120°. The error E_1^i between succesive mesh refinements is computed using the L_1^i norm, which is well suited for the interfacial flow problems:

$$E_1^i = \int_\Omega |H(F_r) - H(F_c)| d\Omega \tag{19}$$

where $H(F)$ is the discontinuous Heaviside function, and F_r and F_c are solutions from, respectively, refined and coarse grids. For the numerical integration of Eq. 19, a domain of 1000x1000 mesh points was used and the solution was interpolated from the actual domain to the computational one. The results obtained are shown in Table 2. As can be seen, increasing the resolution of the grid leads to a decrease in computation error.

Table 1: Physical properties of the fluids.

Property	Density kg/m^3	Viscosity Ns/m^2	Surface Tension N/m
liquid	1000	0.001	0.072
gas	1.225	0.0000178	

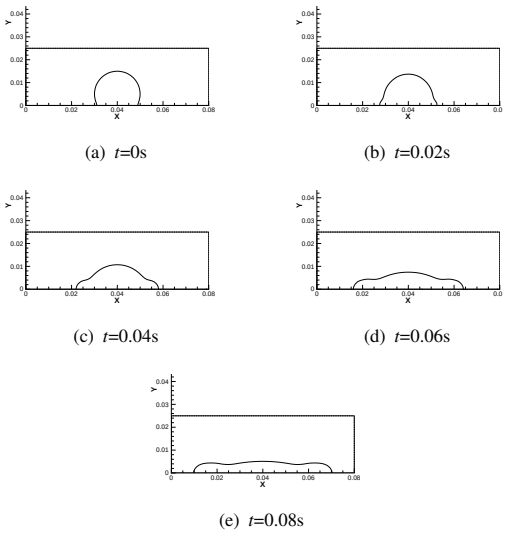

(a) t=0s (b) t=0.02s (c) t=0.04s (d) t=0.06s (e) t=0.08s

Figure 4: Snapshots of the 2D water drop for a grid of 80x25 and gravity vector (0.0,-9.81).

Table 2: Error between successive mesh refinements for 2D air-water simulations with gravity vector (0,-9.81) and (-9.81,0).

Grid	Case 1, E_1^i, $(0, -9.81)$	Case 2, E_1^i, $(-9.81, 0)$
80x25	N.A.	N.A.
160x50	1.22e-2	7.049e-3
320x100	3.359e-3	2.829e-3

The second simulated case was similar to the above, however the gravity vector is (-9.81,0)m/s^2. Thus we

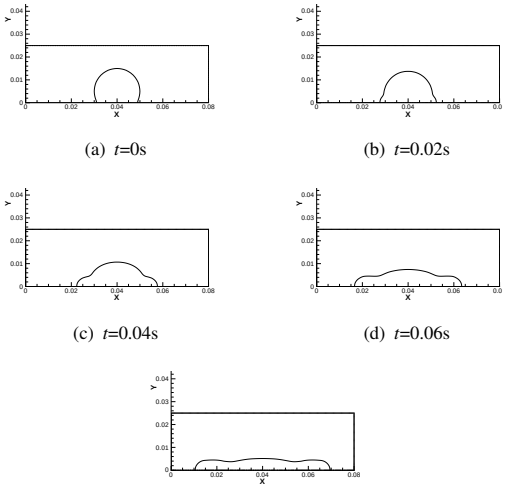

(a) t=0s (b) t=0.02s

(c) t=0.04s (d) t=0.06s

(e) t=0.08s

Figure 5: Snapshots of the 2D water drop for a grid of 160x50 and gravity vector (0.0,-9.81).

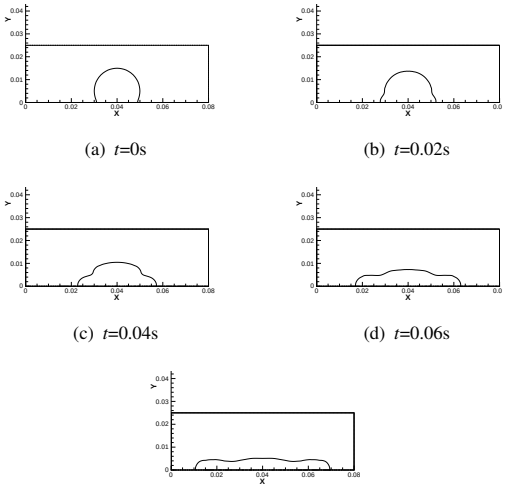

(a) t=0s (b) t=0.02s

(c) t=0.04s (d) t=0.06s

(e) t=0.08s

Figure 6: Snapshots of the 2D water drop for a grid of 320x100 and gravity vector (0.0,-9.81).

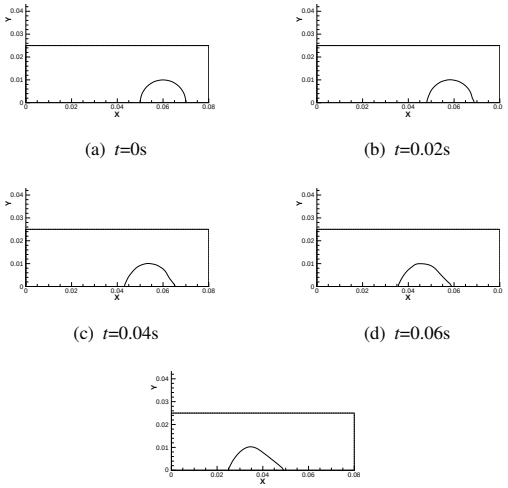

(a) t=0s (b) t=0.02s

(c) t=0.04s (d) t=0.06s

(e) t=0.08s

Figure 7: Snapshots of the 2D bubble contour for a grid of 80x25 and gravity vector (-9.81,0).

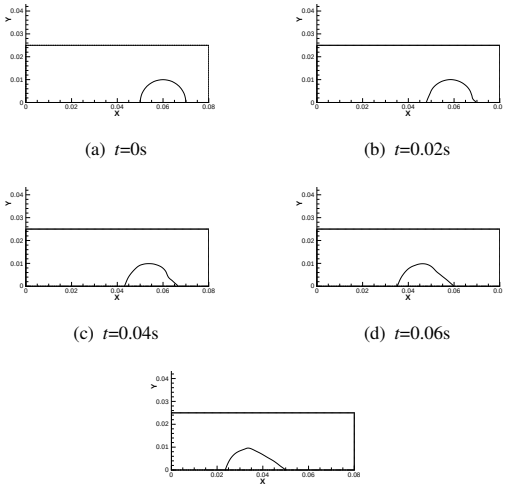

(a) t=0s (b) t=0.02s

(c) t=0.04s (d) t=0.06s

(e) t=0.08s

Figure 8: Snapshots of the 2D bubble contour for a grid of 160x50 and gravity vector (-9.81,0).

expect now to see different contact angles at the two droplet extremities, using the same boundary conditions as in the previous case and three different grids: 80x25, 160x50 and 320x100. Once again the error decreased with increasing mesh densities. Fig 7 shows the droplet contour at different times using a grid of 80x25. As can be seen, the drop moves from right to left under the action of gravity. Fig. 8 and Fig. 9 show the bubble contour on grids of 160x50 and on a grid of 320x100, respectively. The error E_1^i between succesive mesh refinements is computed as is explained above, and the results are shown in Table 2.

3D examples. In this section we extend the 2D examples shown above to the 3D case. For the first case a semi-spherical droplet of 2cm diameter is placed on a wall of a parallelipipedic domain of 8x2.5x8 cm at (4.0,0.5,4.0) cm. Based on the convergence study carried out for the 2D case, the grid chosen was 160x50x160. A no slip wall boundary condition was used for all boundaries. The dynamic contact angle, limited by 65° and 105°, was computed and prescribed at the bottom boundary. Fig. 10 shows the bubble contour in the *XY* plane for *Z*=0.04m at different times. Again good agreement was found when compared with numer-

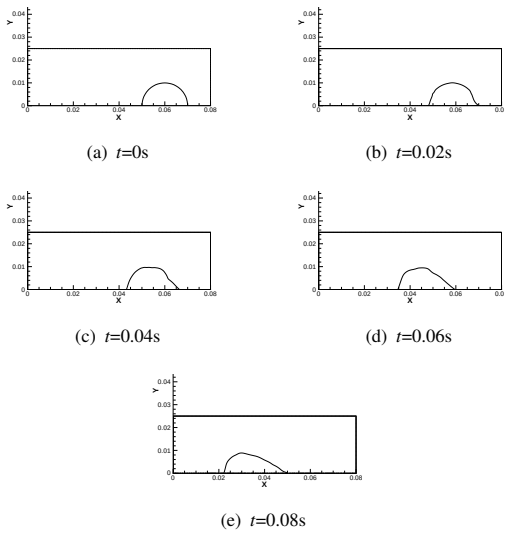

(a) t=0s (b) t=0.02s

(c) t=0.04s (d) t=0.06s

(e) t=0.08s

Figure 9: Snapshots of the 2D bubble contour for a grid of 320x100 and gravity vector (-9.81,0).

ical results of Manservisi and Scardovelli (Manservisi & Scardovelli 2008), and when compared with experimental data of Lim *et al.* (Lim *et al.* 2008) and Grundke *et al.* (Grundke *et al.* 2008).

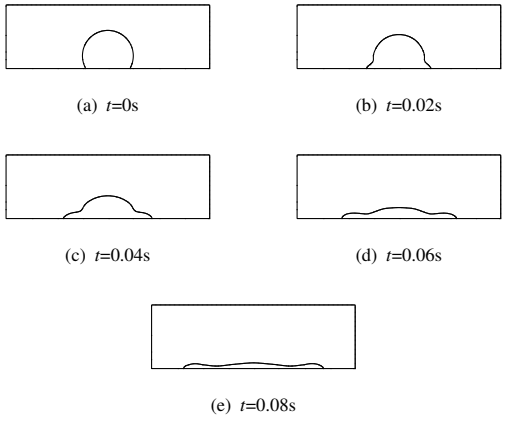

(a) t=0s (b) t=0.02s

(c) t=0.04s (d) t=0.06s

(e) t=0.08s

Figure 10: Snapshots of the 3D bubble contour for a grid of 160x50x160 and gravity vector (0,-9.81,0.0) in plane z=0.04m.

As for the 2D case, the gravity vector was then changed from (0.0,-9.81,0.0) to (-9.81,0.0,0.0). A semi-spherical droplet of 2cm diameter was placed on a wall of a parallelipipedic domain of 8x2.5x8 cm at (4.0,0.0,4.0) cm using a grid of 160x50x160. A no slip wall boundary condition was used for all boundaries. The dynamic contact angle, limited by $65°$ and $105°$, was prescribed at the bottom boundary. Again different contact angles at the droplet extremities were expected. Fig. 11 shows how the shape and position of the droplet changed with time.

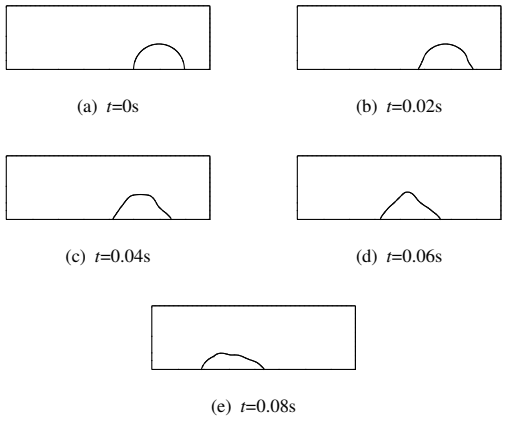

(a) t=0s (b) t=0.02s

(c) t=0.04s (d) t=0.06s

(e) t=0.08s

Figure 11: Snapshots of the 3D bubble contour for a grid of 160x50x160 and gravity vector (-9.81,0.0,0.0) in plane z=0.04m.

Conclusions

The commercial CFD code FLUENT allows one to use a static contact angle between the interface and the wall. In dynamic conditions (i.e. when the contact line starts to move), this choice of a static value is not physically appropriate. Therefore, a dynamic contact angle model was developed and implemented via UDF into the commercial CFD code FLUENT for two phase flows with wetted boundaries.

As a first step, the interface is reconstructed based on the volume fractions. After the interface position is determined, the contact angle is determined based on the volume fractions and the normal to the interface. The model has as its lower limit for the contact angle, the receding contact angle, and as its upper limit, the advancing contact angle. The advancing and receding contact angles are available experimentally for several pairs of fluids/surfaces, or can be estimated using several published correlations.

Several 2D and 3D tests were performed for air/water on a coated silicon wafer surface with different gravity vectors, which proved the accuracy of our model when compared to both numerically and experimentally data available in the literature.

References

J. Brackbill, D. Kothe, C. Zemach, A Continuum Method for Modeling Surface Tension, Journal of Computational Physics 100 (1992) 335–354.

J. Donea, Arbitrary Lagrangian-Eulerian finite element methods, Computational Methods for Transient Analisys 1 (1983) 473–516.

C. Fang, C. Hidrovo, F. Wang, J. Eaton, K. Goodson, 3-D numerical simulation of contact angle hysteresis for microscale two phase flow, International Journal of Multiphase Flow 34 (2008) 690–705.

K. Grundke, S. Michel, G. Knispel, A. Grundler, Wettability of silicone and polyether impression materials: Characterization by surface tension and contact angles measurements, Colloids and Surfaces A: Physicochemical and Engineering Aspects 317 (2008) 598–609.

D. Gueyffier, J. Li, A. Nadim, R. Scardovelli, S. Zaleski, Volume-of-Fluid Interface Tracking with Smoothed Surface Stress Methods for Three-Dimensional Flows, Journal of Computational Physics 152 (1999) 423–456.

F. Harlow, J. Welch, Numerical Calculation of Time-Dependent Viscous Incompressible Flow of Fluid with Free Surface, Physics of Fluids 8 (1965) 2182–2189.

C. Hirt, A. Amsden, J. Cook, An arbitrary Lagrangian-Eulerian computing method for all flow speeds, Journal of Computational Physcs 135 (1997) 203–216.

C. Hirt, B. Nichols, Volume of fluid (VOF) method for the dynamics of free boundaries, Journal of Computational Physics 39 (1981) 201–225.

T. Hughes, W. Liu, T. Zimmermann, Lagrangian Eulerian finite element formulation for incompressible viscous flow, Computer Methods in Applied Mechanics and Engineering 29 (1981) 239–349.

T.-S. Jiang, S.-G. Oh, J. C. Slattery, Correlation for Dynamic Contact Angle, Journal of Colloid and lnterface Science 69 (1979) 74–77.

J. Li, Piecewise Linear Interface Calculation, Comptes Rendus de l'Academie des Sciences Serie II. Fascicule B - Mecanique 320 (1995) 391–396.

T. Lim, S. Han, J. Chung, J. T. Chung, S. Ko, Experimental study on spreading and evaporation of inkjet printed pico-liter droplet on a heated substrate, International Journal of Heat and Mass Transfer.

S. Manservisi, R. Scardovelli, A variational approach to the contact angle dynamics of spreading droplets, Computers & Fluids.

W. F. Noh, P. Woodward, SLIC (Simple Line Interface Calculation), in: Proceeding of the Fifth International Conference on Numerical Methods on Fluid Dynamics, vol. 59 of Lecture Notes in Physics, Springer, 1976.

R. Scardovelli, S. Zaleski, Direct numerical simulation of free surface and interfacial flow, Annual Review of Fluid Mechanics 31 (1999) 657–603.

R. Scardovelli, S. Zaleski, Analytical Relations Connecting Linear Interfaces and Volume Fractions in Rectangular Grids, Journal of Computational Physics 164 (2000) 228–237.

M. Sussman, A. S. Almgren, J. B. Bell, P. Colella, L. H. Howell, M. L. Welcome, An Adaptive Level Set Approach for Incompressible Two Phase Flows, Journal of Computational Physics 148 (1999) 81–124.

M. Sussman, E. Fatemi, An efficient interface-preserving level set redistancing algorithm and its application to interfacial incompressible fluid flow, SIAM Journal on Scientific Computing 20 (4) (1999) 1165–1191.

M. Sussman, E. Fatemi, P. Smereka, S. Osher, An improved level set method for incompressible two-phase flows, Computers & Fluids 27 (5–6) (1998) 663–680.

M. Sussman, P. Smereka, S. Osher, A level set approach for computing solutions to incompressible two-phase flow, Journal of Computational Physics 114 (1994) 146–159.

L. H. Tanner, The spreading of silicone oil drops on horizontal surfaces, Journal of Physics D: Applied Physics 12 (1979) 1473–1484.

G. Tryggvason, B. Bunner, A. Esmaeeli, D. Juric, N. Al-Rawahi, W. Tauber, J. Han, S. Nas, Y.-J. Jan, A Front Tracking Method for the Computations of Multiphase Flow, Journal of Computational Physics 169 (2001) 708–759.

S. O. Unverdi, G. Tryggvason, A Front Tracking Method for Viscous, Incompressible, Multi – fluid Flows, Journal of Computational Physics 100 (1992) 25–37.

D. Youngs, Time dependent multimaterial flow with large fluid distortion, in: K. Morton, M. Baines (eds.), Numerical Methods for Fluid Dynamics, Academic Press, New York, 1982, pp. 273–285.